Harvesting Energy from the Natural Vibration of Human Walking

Weiqing Yang,[†,‡,¶] Jun Chen,[†,¶] Guang Zhu,[†] Jin Yang,[†] Peng Bai,[†] Yuanjie Su,[†,‡] Qingsheng Jing,[†] Xia Cao,[§,⊥,*] and Zhong Lin Wang[†,⊥,*]

[†]School of Materials Science and Engineering, Georgia Institute of Technology, Atlanta, Georgia 30332-0245, United States, [‡]State Key Laboratory of Electronic Thin films and Integrated Devices, University of Electronic Science and Technology of China, Chengdu 610054, China, [§]School of Biochemical and Pharmaceutical Sciences, Capital Medical University, Beijing, 100069, China, and [⊥]Beijing Institute of Nanoenergy and Nanosystems, Chinese Academy of Sciences, Beijing, 100083, China. [¶]Authors with equal contribution.

ABSTRACT The triboelectric nanogenerator (TENG), a unique technology for harvesting ambient mechanical energy based on the triboelectric effect, has been proven to be a cost-effective, simple, and robust approach for self-powered systems. However, a general challenge is that the output current is usually low. Here, we demonstrated a rationally designed TENG with integrated rhombic gridding, which greatly improved the total current output owing to the structurally multiplied unit cells connected in parallel. With the hybridization of both the contact-separation mode and sliding electrification mode among nanowire arrays and nanopores fabricated onto the surfaces of two contact plates, the newly designed TENG produces an open-circuit voltage up to 428 V, and a short-circuit current of 1.395 mA with the peak power density of 30.7 W/m^2. Relying on the TENG, a self-powered backpack was developed with a vibration-to-electric energy conversion efficiency up to 10.62($\pm$1.19) %. And it was also demonstrated as a direct power source for instantaneously lighting 40 commercial light-emitting diodes by harvesting the vibration energy from natural human walking. The newly designed TENG can be a mobile power source for field engineers, explorers, and disaster-relief workers.

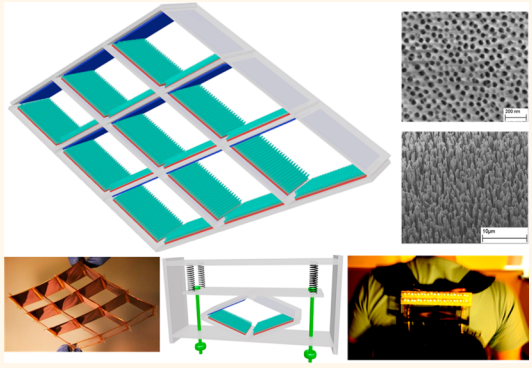

KEYWORDS: triboelectric nanogenerator · rhombic gridding structure · self-powered backpack · human walking

Over the past decades, increasing research efforts have been devoted to harvesting ambient environmental energy owing to the rapid-growing worldwide energy consumptions. The search for clean and renewable energy with reduced carbon emission is urgent to the sustainable development of human civilization. Nowadays people have become increasingly reliant on mobile electronic devices, such as for the purposes of medical, communication, and positioning systems as one moves around cities or in the remote areas. Presently, all of these devices are powered by batteries, which have a limited energy storage capacity and also add considerable additional weight. More importantly, a battery has limited lifetime, and once it is out of charges, it is "dead". Meanwhile, the human body has numerous potential mechanical energy sources; thus, so far, a lot of portable and renewable human motion-driven self-powdered systems were developed relying on the piezoelectric effect,[1−4] electromagnetic effect,[5−8] electrostatic effect,[9,10] and magnetostrictive effect.[11]

Recently, a triboelectric nanogenerator (TENG), based on the universally known contact electrification effect,[12−19] has been proven to be a cost-effective and robust approach for harvesting ambient environmental energy.[20−28] A periodic contact and separation between two materials with different charge affinities acts as a charge-pump to alternately drive induced electrons to flow between the electrodes through an external load. A key challenge to TENG is its relatively low output current. Here, we presented a rationally designed TENG with integrated rhombic gridding as an effective solution to this problem. The newly designed TENG greatly improved the total current output as well as the vibration-to-electric energy conversion efficiency owing to its structurally multiplied unit cells connected in parallel. With the hybridization of

* Address correspondence to zlwang@gatech.edu, caoxia@ccmu.edu.cn.

Received for review October 4, 2013 and accepted November 1, 2013.

Published online 10.1021/nn405175z

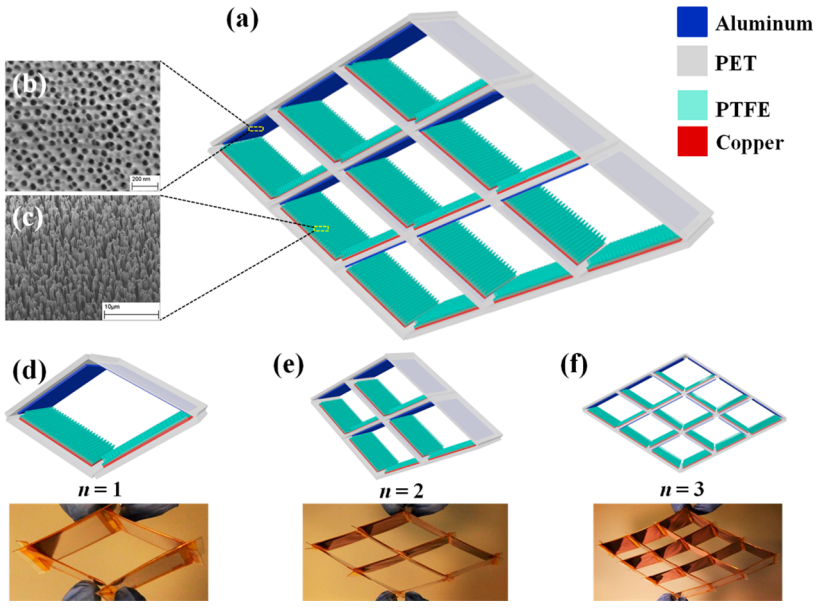

Figure 1. Integrated rhombic gridding based triboelectric nanogenerator. (a) Sketch of a typical TENG with n = 3. (b) SEM image of nanopores on aluminum electrode. (c) SEM image of PTFE nanowires. (d–f) Sketch and corresponding photograph of integrated rhombic gridding based TENG with n = 1, 2, 3, respectively.

both contact and sliding electrification among polytetrafluoroethylene (PTFE) nanowire arrays and aluminum nanopores, the open-circuit voltage (V_{OC}) and short-circuit current density (I_{SC}) of the TENG reach up to 428 V and 36.6 mA/m^2, respectively, with peak power density of 30.7 W/m^2. On the basis of this result, a self-powered backpack was developed. Under the circumstance of natural human walking with loads of 2.0 kg, the power generated by one unit cell is high enough to simultaneously light more than 40 commercial LEDs, rendering a vibration-to-electric energy conversion efficiency up to 10.62 (±1.19) %, which unambiguously demonstrated the capability of our integrated rhombic gridding based TENG acting as a sustainable power source for mobile electronics.

SYSTEM DESIGN AND CHARACTERIZATION

The structure of integrated rhombic gridding based TENG is shown in Figure 1a, in which, the total number of unit cells in one TENG can be expressed as:

$$N_{total} = 2n^2 \quad (1)$$

where n is the number of unit cells along the edge length. The plastic sheets of polyethylene terephthalate (PET) with a thickness of 600 μm are utilized. Each PET sheet is cut half through (Supporting Information, Figure S1) and then locked into each other to form the framework of the TENG. On one side of the PET substrate, an aluminum thin film with nanoporous modification plays dual roles as a contact electrode and a contact surface. A scanning electron microscopy (SEM) image of the aluminum nanopores is shown in Figure 1b. A layer of PTFE film with nanowire arrays was adhered onto the other side of the PET substrate with deposited copper thin film as back electrode. An SEM image of PTFE nanowire arrays is presented in Figure 1c. As demonstrated in Figure 1(d–f), there are 2, 8, and 18 unit cells in the TENGs (sketch and corresponding photograph of real devices) with n = 1, 2, and 3, respectively. This integrated rhombic gridding structure, with unit cells electrically connecting in parallel, is capable of improving the current output with multifold enhancement. Furthermore, the structural coupling of aluminum nanoporous and PTFE nanowires arrays dramatically increases the effective contact area of the TENG. Detailed fabrication specifications are shown in the Experimental Section.

TENG generally has two working modes: contact-separation mode and lateral sliding mode. The currently designed TENG works on the basis of a hybridization of the two modes. A cycle of electricity generation process is illustrated in Figure 2. Because of the coupling of the triboelectric effect and electrostatic induction effect,[12–28] a periodic contact and separation between two materials with opposite triboelectric polarities alternatingly drives induced electrons through an external circuit. According to the triboelectric series,[29] a list of materials based on their tendency to gain or loose charges, electrons are injected from an aluminum electrode into PTFE at the original position (Figure 2a),[13,20–22,30] resulting in positive charges at the surface of the PTFE film and negative charges at the aluminum electrode. Once a periodic external force acts on the TENG, a separation of the two plates forms with an included angle of θ, as shown in Figure 2b, producing an electric potential difference between the contact electrode and back electrode. As demonstrated in Supporting Information, Figure S2, according to the Gauss Theorem, the electric

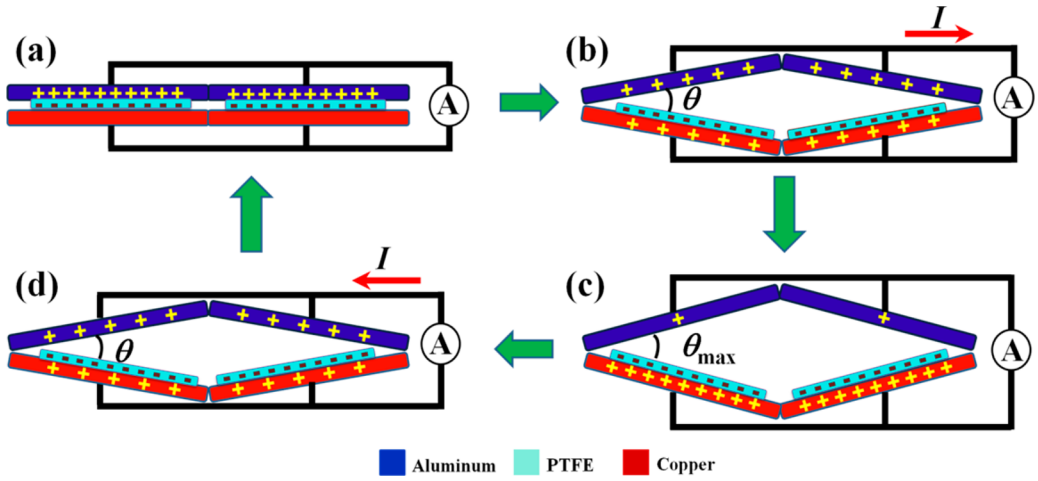

Figure 2. Sketch that illustrates the operating principle of the integrated rhombic gridding based TENG. (a) Original position of TENG. Positive and negative triboelectric charges are generated on the aluminum side and the PTFE side, respectively. (b) The applied external force causes a separation. Electric potential difference drives electrons flowing from the back electrode to the contact electrode. (c) The included angle of the plates reaches its maximum and so do the induced charges. (d) Electrons are driven back from the contact electrode to the back electrode due to the decreased separation.

potential deference of the two electrodes can be expressed as

$$V_A - V_B = \int_A^C \left(\frac{\sigma - \Delta\sigma}{2\varepsilon_0} + \frac{\sigma}{2\varepsilon_0} - \frac{\Delta\sigma}{2\varepsilon_0}\right) dl + \int_C^B \left(\frac{\sigma - \Delta\sigma}{2\varepsilon_0\varepsilon_r} - \frac{\sigma}{2\varepsilon_0\varepsilon_r} - \frac{\Delta\sigma}{2\varepsilon_0\varepsilon_r}\right) dl \quad (2)$$

where V_A and V_B are the electric potential of the contact electrode and back electrode, respectively. σ is the triboelectric charge density, $\Delta\sigma$ is the induced charge density, ε_0 and ε_r is the vacuum permittivity and the relative permittivity of PTFE, respectively. If the device is in the open-circuit state, there are no transferring induced charges, that is,

$$\Delta\sigma = 0 \quad (3)$$

So, the open circuit voltage can be calculated as (see Supporting Information for detailed derivation of the analytical model):

$$V_{oc} = \frac{2\sigma l \sin\frac{\theta}{2}}{\varepsilon_0} \quad (4)$$

where l is the edge length of one rhombic unit cell. If the device is in the short-circuit state, the electric potential deference of the two electrodes becomes zero,

$$V_A - V_B = 0 \quad (5)$$

The transferred induced charge density of the TENG can be shown as

$$\Delta\sigma = \frac{\sigma}{1 + \frac{d_1}{2\varepsilon_r l \sin(\theta/2)}} \quad (6)$$

where d_1 is the thickness of PTFE. So, the short-circuit current can be expressed as (see Supporting Information for detailed derivation of the analytical model)

$$I_{SC} = \frac{\sigma s d_1 v}{\varepsilon_r \left[2l\sin\left(\frac{\theta}{2}\right) + \frac{d_1}{\varepsilon_r}\right]^2} \quad (7)$$

where v is the relative velocity of the two contact plates whose motion direction determine the motion direction of the induced charge, thus, the direction of the short circuit current; s is the effective contact area. Such a raise of the electric potential difference drives electrons from the back electrode to the contact electrode through the external circuit, screening the positive triboelectric charges on the back electrode (Figure 2b). When the included angle reaches its maximum θ_{max}, the positive triboelectric charges are nearly completely neutralized by the inductive electrons (Figure 2c). Once the external force acts on the TENG again, the decreasing of electric potential difference drives the inductive electrons to move in a reversed direction (Figure 2d). The process shown in Figure 2(a−d) is a complete cycle of electricity generation. And the TENG acts as an electron-pump that drives electrons back and forth flowing between two electrodes, producing an alternating current in the external circuit.

On the basis of eq 7, various factors, such as the charge density σ, the effective contact area s, and the relative velocity v of the contact or separation of two plates, determine the short circuit current of TENG. Also it can be tuned from following aspects: (i) Selection of contact electrification materials. The triboeletric charge density σ is largely determined by the charge affinity difference of two contact materials.[31,32] Of all materials, PTFE is so far the most electronegative with a charge affinity of −190 nC/J, which was tested by Bill Lee (see Tables 1 and 2 of Supporting Information). Moreover, being electropositive, the charge affinity of

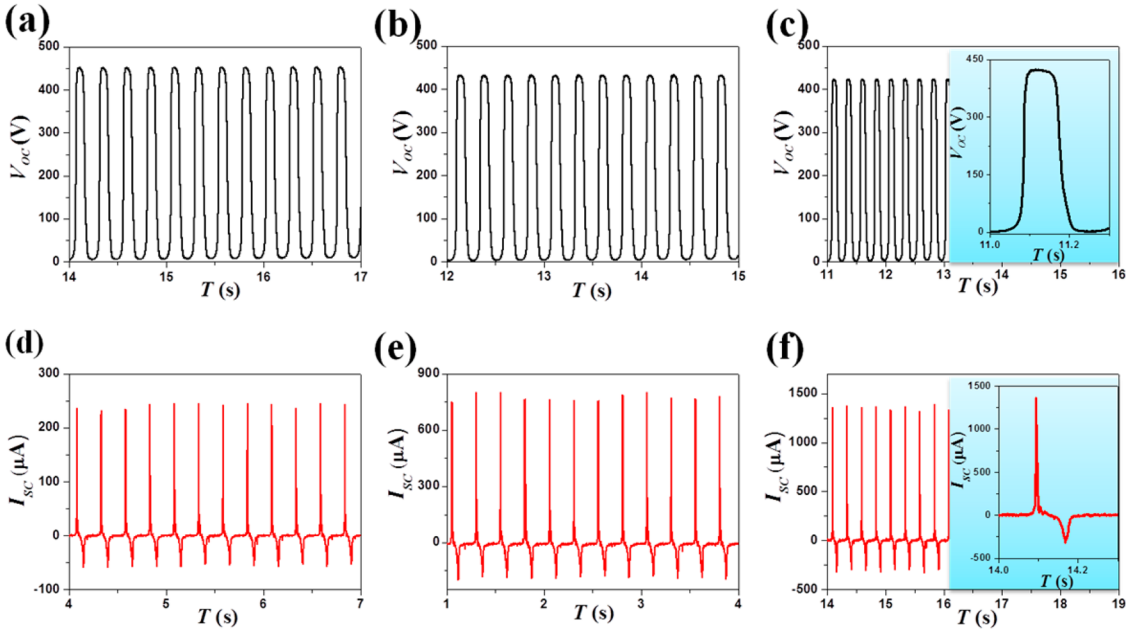

Figure 3. Electrical measurement of the integrated rhombic gridding based TENG. Open-circuit voltage (V_{OC}) (a,b,c) and short-circuit current (I_{SC}) (d,e,f) of the TENG with n = 1, 2, and 3, respectively. Insets of panels c and f are enlarged views of V_{OC} and I_{SC} in one cycle for the TENG with n = 3, respectively.

aluminum is about 10−30 nC/J.[31,32] So large charge affinity difference assures the high generation of triboelectric charges and thus a superior electric output of our device. (ii) Surface modification by nanomaterials. The nanomaterials-based surface modification can greatly enhance the effective contact area *s*. A detailed discussion is provided in Supporting Information. (iii) Relative velocity of surface contact and separation. The periodical contact and separation of the contact surfaces acts as an electron pump to drive the induced charges back and forth, producing alternating current in the external circuit.

RESULTS AND DISCUSSION

To enhance the total current output of the TENG, all of the unit cells are electrically connected in parallel. Under the fixed triggering frequencies and amplitude, the electric output measurement was performed on the integrated rhombic gridding based TENG with n = 1, 2, 3 (Figure 3). The effective contact area of TENG is $2n^2 \times 4.6$ cm $\times$ 4.6 cm, which produces an open-circuit voltages (V_{OC}) 445 V at n = 1 (Figure 3a), 439 V at n = 2 (Figure 3b), and 428 V at n = 3 (Figure 3c). The voltage output is almost constant for all the measurements because all of the rhombic unit cells are electrically connected in parallel. As shown in the inset of Figure 3c, a positive voltage peak is generated due to the immediate charge separation at the departure of aluminum from PTFE. Since the electrons cannot flow back to screen the induced electric potential difference between the two electrodes under the open-circuit condition, the voltage holds at a plateau until the next contact emerges.[20−28] Meanwhile, the peak values of the short-circuit current (I_{SC}) reach up to 245 μA at n = 1 (Figure 3d), 801 μA at n = 2 (Figure 3e), and 1.395 mA at n = 3 (Figure 3f). In addition, as shown in the inset of Figure 3f, the output current has an alternating behavior with asymmetrical amplitudes, with the larger peaks corresponding to the process in which the two contact surfaces move toward each other, while the smaller ones are generated as the two surfaces move apart. According to eq 7, the faster approach is expected to produce larger current peaks than the slower separation.

As indicated in Figure 4a, the current enhancement factor α is a function of the number of unit cells along the edge length, $\alpha = bn^2$. The fitting result renders the coefficient b a value of 1.66. Considering the nonideal experimental factors, such as humidity, particle contaminations in the air, the imperfection from the device fabrication process, and the difficulty of synchronizing of all the device units, which may potentially have negative impact on the actual output, the experimental result of the enhancement factor is considerably approaching the ideal value of $2n^2$ (see Supporting Information for detailed explanation), revealing that the integrated rhombic gridding structure can effectively enhance the total current output. As illustrated in Figure 4b, the accumulative induced charges increase with n, which reaches up to 142.68 μC within 2.75 s when n = 3, further indicating that the integrated rhombic gridding structure can dramatically enhance the electric output of TENG. It is noteworthy that the accumulative induced charges are the sum of all the back-and-forth induced charges in the entire process of the TENG working as a "charge pump".

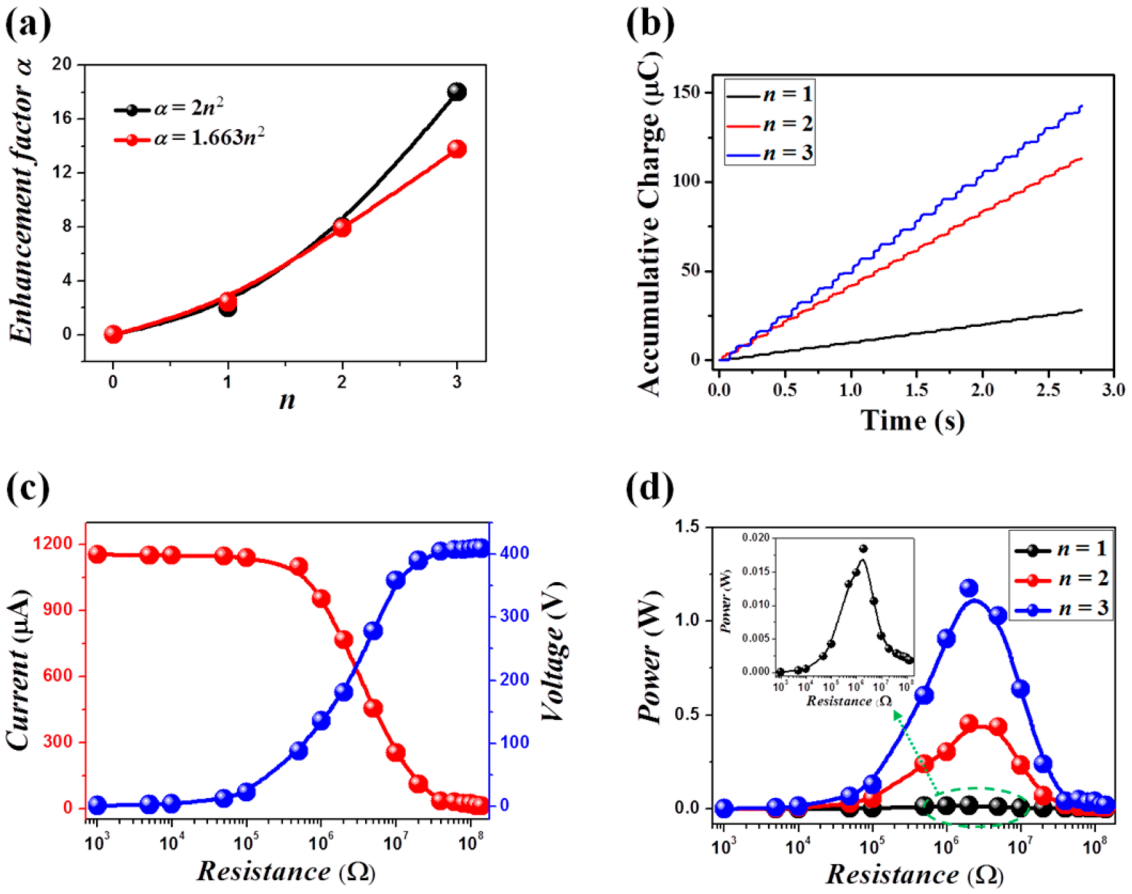

Figure 4. Electrical measurement of the integrated rhombic gridding based TENG. (a) The current's enhancement factor α is increasing as a function of number of unit cells along the edge length *n*. (b) Accumulative inductive charges generated by the TENG with *n* = 1, 2 and 3, respectively. (c) Dependence of the voltage and current output on the external load resistance for the TENG with *n* = 3. The lines are the fitted results. (d) Dependence of the peak power output on the resistance of the external load for the TENG with *n* = 1, 2, and 3, indicating maximum power output obtained at *R* = 2 MΩ. The curve is fitted result. Inset: an enlarged view of peak power output with *n* = 1.

Consequently, it is a monotonically increasing function of time throughout our experimental time window.

Resistors were utilized as external loads to further investigate the output power of the integrated rhombic gridding based TENG with $n = 3$. As displayed in Figure 4c, the current amplitude drops with increasing load resistance owing to the Ohmic loss, while the voltage follows a reverse trend. Similar trends for $n = 1$ and 2 are presented in Supporting Information, Figure S3. As demonstrated in Figure 4d, all of the instantaneous peak power ($I^2_{peak}R$) for $n = 1$, 2, and 3 are maximized at a load resistance of 2 MΩ. Moreover, the peak power dramatically increases with the increase of n, which reaches up to 1.17 W at $n = 3$, corresponding to the peak power density and volumetric energy density of 30.7 W/m^2 and 1.54 × 10^4 W/m^3, respectively. In addition, the robustness is another critical criterion for the TENG devices. As demonstrated in Supporting Information, Figure S4, only a slight drop of about 5% is observed for the short-circuit current after more than 0.1 million cycles of vibration.

The integrated rhombic gridding based TENG demonstrated here has three unique characteristics. First, by using the novel integrated rhombic gridding structure, the total number N of unit cells, which are electrically connected in parallel, theoretically follows a rule of $N = 2n^2$. This is the key factor of dramatically enhancing the total electric output. Second, to promote the triboelectrification and to increase the effective contact area between the two contact surfaces, aluminum nanopores and PTFE nanowires are simultaneously created as surface modifications. The rational design, coupled with nanomaterial modification, greatly increases the effective contact area and thus the triboelectric charges (please see the further discussion in Figure S5 of Supporting Information). Lastly, the structural coupling of nanopores and nanowire can also enhance the triboelectrification process for TENGs. As a comparison, the electric measurement of TENG ($n = 1$) without surface modification is shown in Supporting Information, Figure S6, indicating that the short circuit current output with nanostructure modification is about 2.8 times of that without surface modification. In addition, it is worth noting that, as a consummative integration of the contact electrification effect, electrostatic induction, and kinetic effect as well as

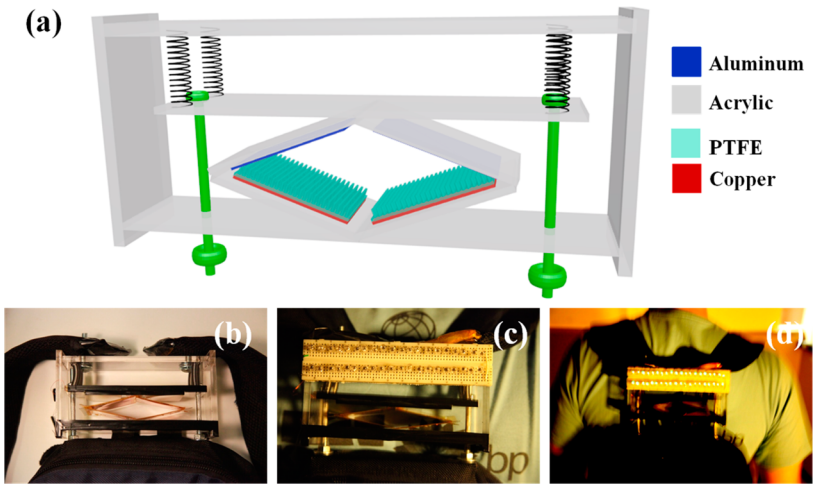

Figure 5. (a, b) Sketch and photograph of a self-powered backpack which has been developed on the basis of the integrated rhombic gridding based TENG. (c) Photograph of the backpack on the shoulder with human standing still. (d) Photograph of the backpack under normal human walking. Forty commercial LED bulbs were lit simultaneously.

nanotechnology, this newly invented TENG cannot be simply considered as the traditional electrets, which is dielectric material exhibiting a quasi-permanent electric charge *via* the "pre-charging" processing from an external electric field.[32−38]

To prove the capability of the integrated rhombic gridding based TENG as a sustainable power source, a backpack was developed to harvest vibration energy from natural human walking. As indicated in Figure 5a, four acrylics plates were built into a supporting shelf with a size of 5 cm × 7.5 cm × 20 cm, which bridged the backpack and its two straps using four springs and two long screw shanks. The integrated rhombic gridding based TENG with n = 1 is sandwiched between two acrylic sheets and the photograph of a real backpack is shown in Figure 5b. A total of forty commercial LED bulbs were assembled in series on a piece of electric board (Figure 5c), electrically connected to the newly designed backpack. When a person walks naturally carrying the designed backpack with a total weight of 2.0 kg, the power harvested from the body vibration is high enough to simultaneously light all the 40 LEDs (see Figure 5d and the Supporting video).

As an important figure of merit, we investigated the vibration-to-electric energy conversion efficiency of the self-powered backpack. The conversion efficiency η_{direct} is defined as the ratio of the electric energy delivered to the vibration energy of the backpack triggered by human walking. And the electric energy delivered by the TENG can be expressed as (Supporting Information, Figure S7),

$$E_{electric} = Q = \int_{t_1}^{t_2} I^2 R\, dt = R \int_{5.8217}^{5.8489} I^2\, dt = 3.18\ \text{mJ} \quad (8)$$

where Q is the Joule heating energy, I is the instantaneous current, and R is the load resistance, which is 2 MΩ in the experimental measurement. In the course of backpack vibration, its gravitational potential energy (E_G) is mainly converted into two parts, the elastic potential energy ($E_{elastic}$) and electric energy. The gravitational potential energy and elastic energy can be estimated as following,

$$E_G = mg\Delta x = 2.0\ \text{kg} \times 9.8\ \text{N/kg} \times 0.015\ \text{m} = 294\ \text{mJ} \quad (9)$$

$$E_{elastic} = \frac{1}{2} k\Delta x^2 N = 264.09\ \text{mJ} \quad (10)$$

where m is the total weight of the backpack, Δx is the average displacement of each spring, which was measured from the supporting video processing; k is the spring stiffness factor (k = 586.86 N/m), and N is the number of springs (N = 4). Since the elastic energy stored in the springs has no loss during the backpack vibration, the direct energy conversion efficiency can be calculated as

$$\eta_{direct} = \frac{E_{electric}}{E_G - E_{elastic}} \times 100\% = 10.6\% \quad (11)$$

Likewise, we repeatedly measured the energy conversion efficiency 10 times and an averaged value of 10.62(±1.19)% was thus obtained. Such high energy conversion efficiency of the TENG enables tremendous potential applications for powering some small electronics by harvesting the vibration energy from human motions.

CONCLUSIONS

We demonstrated a novel integrated rhombic gridding based TENG. This innovative structure provides $2n^2$ unit cells electrically connected in parallel, which is able to greatly enhance the current output as well as the vibration-to-electric energy conversion efficiency. Also, the surface modification by PTFE nanowire-arrays

and aluminum nanopores renders a hybridization of both contact-separation and lateral sliding electrification modes for effectively improving the electric output. The newly designed TENG with $n = 3$ produces an open-circuit voltage up to 428 V, and a short-circuit current of 1.395 mA with a peak power density of 30.7 W/m^2. The electric output is related to n and increases manifoldly as a function of $2n^2$. Moreover, based on the TENG, a self-powered backpack was developed with a considerably high vibration-to-electric energy conversion efficiency of 10.62(±1.19)%. When a person walks naturally carrying the designed backpack with a total weight of 2.0 kg, the power harvested from the body vibration is high enough to simultaneously light all the 40 LEDs. Our newly designed TENG provides an innovative approach to effectively enhance the device current output and thus it is capable of harvesting vibration energy from natural human walking, which can have a range of applications for extending the lifetime of a battery as well as the possibility of replacing a battery for building self-powered systems.

EXPERIMENTAL SECTION

Fabrication of a Honeycomb-Based TENG. The plastic sheets of polyethylene terephthalate (PET) (McMaster-Carr Company) with a size of $n \times 5.0$ cm $\times$ 5.0 cm $\times$ 0.6 mm ($n = 1, 2, 3$) act as the flexible supporting substrates of TENG. Each PET sheet is cut half through and then locked into each other to form the framework of the TENG. On the one side of the PET substrate, aluminum thin film with a nanoporous surface acts as both contact electrode and contact surface. A layer of polytetrafluoroethylene (PTFE) film with nanowires arrays was adhered onto the other side of the PET substrate with deposited copper as back electrode.

Nanopore-Based Aluminum Surface Modification. The electrochemical anodization method was used to create the nanopores on the surface of an aluminum thin film. The mass concentration of oxalic acid ($H_2C_2O_4$) (Sigma Aldrich) electrolyte is 4%, and the electrochemical anodization is made under the bias voltage of 25 V for 5 h with platinum as a cathode. Then the alumina layer was etched away in a solution of 20 g/L chromic acid (Sigma Aldrich) at 60 °C for 2 h.

Nanowire-Based PTFE Surface Modification. A sample of 100 nm Cu-coated PTFE film with a thickness of 50 μm was prepared for the etching process. Then the aligned PTFE nanowires were created onto the PTFE surface *via* the ICP reactive ion etching method. In the etching process, O_2, Ar, and CF_4 gases were injected into the ICP chamber with flow ratios of 10.0, 15.0, and 30.0 sccm, respectively. Plasma with a large density was generated by a power source of 400 W. The plasma ions were accelerated by another applied power of 100 W. The aligned PTFE nanowires with an average length of 1.5 μm were obtained after a 40 s etching process.

Conflict of Interest: The authors declare no competing financial interest.

Acknowledgment. Research was supported by Airforce (MURI), U.S. Department of Energy, Office of Basic Energy Sciences (Award DE-FG02-07ER46394), NSF (0946418), the Knowledge Innovation Program of the Chinese Academy of Science (Grant No. KJCX2-YW-M13), and the "Thousands Talents" program for a pioneer researcher and his innovation team, China. P.B. thanks the support from the Chinese Scholars Council. X.C. thanks the National Natural Science Foundation of China (NSFC No. 21275102) for support. Patents have been filed based on the research results presented in this manuscript.

Supporting Information Available: (1) Sketch of half-cutting through PET plastics sheets as a supporting framework for the integrated rhombic gridding based TENG; (2) analytical model for calculating the open-circuit voltage and short-circuit current of the integrated rhombic gridding based TENG; (3) derivation of the TENG current's enhancement factor; (4) dependence of the voltage and current output on the external load resistance for the TENG with $n = 1$ and 2, respectively; (5) device robustness investigation; (6) investigation of the electric output improvement from surface modification; (7) enlarged view of the current peak which is generated by a person walking naturally carrying the self-powered backpack with a load of 2 kg; (8) supporting video of a self-powered backpack. This material is available free of charge *via* the Internet at http://pubs.acs.org.

REFERENCES AND NOTES

1. Wang, Z. L.; Song, J. H. Piezoelectric Nanogenerators Based on Zinc Oxide Nanowire Arrays. *Science* **2006**, *312*, 242–246.
2. Wang, X. D.; Song, J. H.; Liu, J.; Wang, Z. L. Direct-Current Nanogenerator Driven by Ultrasonic Waves. *Science* **2007**, *316*, 102–105.
3. Qin, Y.; Wang, X.; Wang, Z. L. Microfibre-Nanowire Hybrid Structure for Energy Scavenging. *Nature* **2008**, *451*, 809–813.
4. Yang, R. S.; Qin, Y.; Dai, L. M.; Wang, Z. L. Power Generation with Laterally Packaged Piezoelectric Fine Wires. *Nat. Nanotechnol.* **2008**, *4*, 34–39.
5. Lawrence, C. R.; Louis, F.; Evan, M. G.; Taeseung, D. Y. Generating Electricity while Walking with Loads. *Science* **2005**, *309*, 1725–1728.
6. Bai, X. L.; Wen, Y. M.; Yang, J.; Li, P.; Qiu, J.; Zhu, Y. A Magnetoelectric Energy Harvester with the Magnetic Coupling to Enhance the Output Performance. *J. Appl. Phys.* **2012**, *111*, 07A938−1–3.
7. Ayala-Garcia, I. N.; Zhu, D.; Tudor, M. J.; Beeby, S. P. A Tunable Kinetic Energy Harvester with Dynamic over Range Protection. *Smart Mater. Struct.* **2010**, *19*, 115005–115014.
8. Ayala-Garcia, I. N.; Mitcheson, P. D.; Yeatmanm, E. M.; Zhu, D.; Tudor, J.; Beeby, S. P. Magnetic Tuning of a Kinetic Energy Harvester Using Variable Reluctance. *Sens. Actuators A* **2013**, *189*, 266–275.
9. Mitcheson, P. D.; Miao, P.; Stark, B. H.; Yeatman, E. M.; Holmes, A. S.; Green, T. C. MEMS Electrostatic Micropower Generator for Low Frequency Operation. *Sens. Actuators A* **2004**, *115*, 523–529.
10. Wei, Y.; Yorah, R.; Yang, K.; Beeby, S. P.; Tubor, J. Screen Printing of a Capacitive Cantilever-Based Motion Sensor on Fabric Using a Novel Sacrificial Layer Process for Smart Fabric Applications. *Meas. Sci. Technol.* **2013**, *24*, 075104–075114.
11. Wang, L.; Yuan, F. G. Vibration Energy Harvesting by Magnetostrictive Material. *Smart Mater. Struct.* **2008**, *17*, 045009.
12. Lowell, J.; Roseinnes, A. C. Contact Electrification. *Adv. Phys.* **1980**, *29*, 947–1023.
13. Castle, G. S. P. Contact Charging between Insulators. *J. Electrost.* **1997**, *40−1*, 13–20.
14. Yang, X. H.; Zhu, G.; Wang, S. H.; Zhang, R.; Lin, L.; Wu, W. Z.; Wang, Z. L. A Self-powered Electrochromic Device Driven by a Nanogenerator. *Energy Environ. Sci.* **2012**, *5*, 9462–9466.
15. Horn, R. G.; Smith, D. T. Contact Electrification and Adhesion between Dissimilar Materials. *Science* **1992**, *256*, 362–364.
16. Yang, W. Q.; Chen, J.; Zhu, G.; Wei, X. N.; Bai, P.; Su, Y. J.; Lin, Y.; Wang, Z. L. Harvesting Vibration Energy by a Triple-Cantilever Based Triboelectric Nanogenerator. *Nano Res.* **2013**, 10.1007/s12274-013-0364-0.

17. Horn, R. G.; Smith, D. T.; Grabbe, A. Contact Electrification Induced by Monolayer Modification of a Surface and Relation to Acid–Base Interactions. *Nature* **1993**, *366*, 442–443.
18. Baytekin, H. T.; Patashinskii, A. I.; Branicki, M.; Baytekin, B.; Grzybowski, B. A. The Mosaic Surface Charge in Contact Electrification. *Science* **2011**, *333*, 308–312.
19. Soh, S.; Kwok, S. W.; Liu, H.; Whitesides, G. M. Contact De-electrification of Electrostatically Charged Polymers. *J. Am. Chem. Soc.* **2012**, *134*, 20151–20159.
20. Fan, F. -R.; Tian, Z. -Q.; Wang, Z. L. Flexible Triboelectric Generator. *Nano Energy* **2012**, *1*, 328–334.
21. Fan, F. -R.; Lin, L.; Zhu, G.; Wu, W.; Zhang, R.; Wang, Z. L. Transparent Triboelectric Nanogenerators and Self-Powered Pressure Sensors Based on Micropatterned Plastic Films. *Nano Lett.* **2012**, *12*, 3109–3114.
22. Zhu, G.; Pan, C.; Guo, W.; Chen, C. -Y.; Yu, R.; Wang, Z. L. Triboelectric-Generator-Driven Pulse Electrodeposition for Micropatterning. *Nano Lett.* **2012**, *12*, 4960–4965.
23. Wang, S.; Lin, L.; Wang, Z. L. Nanoscale Triboelectric-Effect-Enabled Energy Conversion for Sustainably Powering Portable Electronics. *Nano Lett.* **2012**, *12*, 6339–6346.
24. Zhu, G.; Lin, Z. -H.; Jing, Q.; Bai, P.; Pan, C.; Yang, Y.; Zhou, Y.; Wang, Z. L. Toward Large-Scale Energy Harvesting by a Nanoparticle-Enhanced Triboelectric Nanogenerator. *Nano Lett.* **2013**, *13*, 847–853.
25. Bai, P.; Zhu, G.; Lin, Z. H.; Jing, Q. S.; Shen, J.; Zhang, G.; Ma, J. S.; Wang, Z. L. Integrated Multipayered Triboelectric Nanogenerator for Harvesting Biomechanical Energy from Human Motions. *ACS Nano* **2013**, *7*, 3713–3719.
26. Zhang, X. S.; Han, M. D.; Wang, R. X.; Zhu, F. Y.; Li, Z. H.; Wang, W.; Zhang, H. X. Frequency-Multiplication High-Output Triboelectric Nanogenerator for Sustainably Powering Biomedical Microsystems. *Nano Lett.* **2013**, *13*, 1168–1172.
27. Zhu, G.; Chen, J.; Liu, Y.; Bai, P.; Zhou, Y. S.; Jing, Q. S.; Pan, C. F.; Wang, Z. L. Linear-Grating Triboelectric Generator Based on Sliding Electrification. *Nano Lett.* **2013**, *13*, 2282–228.
28. Wang, S. -H.; Lin, L.; Xie, Y. N.; Jing, Q. S.; Niu, S. M.; Wang, Z. L. Sliding-Triboelectric Nanogenerators Based on In-Plane Charge Separation Mechanism. *Nano Lett.* **2013**, *13*, 2226–2233.
29. Cross, J. A. *Electrostatics: Principles, Problems and Applications*; Adam Hilger: Bristol, UK, 1987; Chapter 2.
30. Nemeth, E.; Albrecht, V.; Schulert, G.; Simon, F. Polymer Tribo-electric Charging: Dependence on Thermodynamic Surface Properties and Relative Humity. *J. Electrost.* **2003**, *58*, 3–16.
31. Diaz, A. F.; Felix-Navarrro, R. M. A Semi-quantitative Tribo-electric Series for Polymeric Materials: The Influence of Chemical Structure and Properties. *J. Electrost.* **2004**, *62*, 227–290.
32. Sessler, G. M. *Electrets*; Springer-Verlag: Berlin, 1987; Chapter 2.
33. Kestelman, V. N.; Pinchuk, L. S.; Glodade, V. A. *Electrets in Engineering Fundamentals and Applications*; Kluwer Academic Publishers: Boston, MA, 2000; Chapter 1.
34. Hillenbrand, J.; Kodejska, M.; Garcin, Y.; Seggem, H. V.; Sessler, G. M. High-Sensitivity Piezoelectret-Film Accelerometers. *IEEE Trans. Dielectr. Electr. Insul.* **2010**, *17*, 1021–1027.
35. Zhang, X.; Hillenbrand, J.; Sessler, G. M.; Haberzettl, S.; Lou, K. Fluoroethylenepropylene Ferroelectrets with Patterned Microstructure and High, Thermally Stable Piezoelectricity. *Appl. Phys. A: Mater. Sci. Process.* **2012**, *107*, 621–629.
36. Kempitiya, A.; Tasciuc, D. A.; Hella, M. M. Low-Power Interface IC for Triplate Electrostatic Energy Converters. *IEEE Trans. Power Electr.* **2013**, *28*, 609–614.
37. Janicek, V.; Husak, M. Designing the 3D Electrostatic Microgenerator. *J. Electrost.* **2013**, *71*, 214–219.
38. Wada, N.; Mukougawa, K.; Horiuchi, N.; Hiyama, T.; Nakamura, M.; Nagai, A.; Okura, T.; Yamashita, K. Fundamental Electrical Properties of Ceramic Electrets. *Mater. Res. Bull.* **2013**, *48*, 3854–3859.